Linear Paul trap for strontium ions

D. J. Berkeland

Citation: Review of Scientific Instruments **73**, 2856 (2002);
View online: https://doi.org/10.1063/1.1489073
View Table of Contents: http://aip.scitation.org/toc/rsi/73/8
Published by the American Institute of Physics

Linear Paul trap for strontium ions

D. J. Berkeland[a)]
P-23, Physics Division, Los Alamos National Laboratory, Los Alamos, New Mexico 87545

(Received 4 October 2001; accepted for publication 6 May 2002)

We demonstrate a linear radio-frequency trap for confining strontium ions that is simply constructed nearly entirely with commercial off-the-shelf components. The electrodes of this trap are spaced to allow tight radial confinement, and segmented to give tight axial confinement with minimal distortion of the radio-frequency field. The resulting secular frequencies of the trap are 1 MHz in the radial direction and 100 kHz in the axial direction, the ions can be imaged with 2–3 μm resolution, and we detect over 20 000 photons per second per ion. This article describes the construction of the vital parts of the trap system, the laser system and optics used to Doppler cool the ions and to observe quantum jumps, and the operation and behavior of the complete system. © *2002 American Institute of Physics.* [DOI: 10.1063/1.1489073]

I. INTRODUCTION

Paul traps have proven themselves to be indispensable tools for precision measurements,[1] quantum optics,[2] and investigations of quantum computation.[3] This is due to the extreme spatial localization of the ion and its isolation from external perturbations. To further develop these advantages, in recent years linear Paul traps have been developed to confine more than one ion with minimal perturbation from the trap's radio-frequency (rf) field,[4] and several linear Paul traps of millimeter radial dimensions have been used to tightly confine laser-cooled ion crystals. These traps confine ions radially in an oscillating quadratic electric field created by the (typically) rf voltages applied to four parallel trap electrodes, with the ions sitting at or near the nodal line of the rf field. The ions are confined axially by a static potential created by voltages applied to ''end-cap'' electrodes at both ends of the trap. The end-cap electrodes can be independent sections of the parallel trap electrodes,[5–8] separate cylindrical, or conically shaped electrodes that surround the four parallel electrodes,[9–12] conducting plates at either end of the trap and perpendicular to the four parallel electrodes[13] or rods inserted into the trapping region along the trap axis.[14]

The contribution of this work to the field is to show that such trapping systems can be simply and inexpensively built. This article details a miniature linear ion trap that can be constructed with commercial off-the-shelf components. The imaging optics are simple and only a few components of the vacuum chamber and trap system are custom machined. The laser system comprises two external cavity diode lasers and a diode-pumped fiber laser, runs entirely from standard 120 V single-phase power, and does not require any water cooling. It is hoped that this article will show that an ion-trapping system can be set up with minimal use of machine shop time and only common building facilities.

a)Electronic mail: djb@lanl.gov

II. ION TRAP AND VACUUM SYSTEM

Figure 1 shows a schematic diagram of the trap. All electrodes are made of 304 stainless steel. Four parallel 0.79-mm-diam rods, approximately 5 cm long, are arranged with their axial centers on a square that is 1.25 mm on each side. Two diagonally opposite rods are connected to potentials $V_1 = U_1 + V_{\mathrm{rf}} \cos(\Omega t)$ and $V_2 = U_2 + V_{\mathrm{rf}} \cos(\Omega t)$, where $\Omega/2\pi = 7.1$ MHz. These potentials are created by a quarter-wave helical resonator[15] whose coil is made of two twisted wires each connected to one of these rf rods. The loaded Q of this resonator is about 70, and approximately 100 mW of rf power inductively coupled into it gives $V_{\mathrm{rf}} \sim 100$ V. An inexpensive amplifier (Mini-Circuits ZHL-32A) can increase the input power to about a watt to bring V_{rf} up to several hundred volts. The remaining two 5-cm-long rods are held at bias voltages U_3 and U_4. These four rods create an oscillating field that is quadrupolar near the trap axis and confines the ions along the radial direction. The bias voltages U_1, U_2, U_3, and U_4 are adjusted to force the ions to the rf nodal line of the trap, where micromotion is minimized.[16] To confine the ions along the trap axis, two approximately 10-mm-long tube electrodes with 0.88 mm inner diameter and 1.05 mm outer diameter are slipped over the rods that are held at potentials U_3 and U_4. These electrodes are at potential U_0, creating a static quadratic potential along the trap axis.

The tube electrodes are formed by cutting and grinding a longer stainless tube with a Dremmel tool. They are insulated from the rod electrodes by polyimide tubes whose wall thickness is 25 μm. These insulating tubes are completely covered by the stainless tubes to shield the trap region from stray voltages due to any charges on the polyimide. The assembly is tightly fitted together and held in place by friction. Connections to the rod electrodes are made by simply spot welding 0.25-mm-diam stainless-steel wire to their ends. Spot welding to the tube electrodes without significantly denting them proved difficult, so tabs several mm long were carved into the tube ends and the wires were spot welded to these tabs. Each dc biased electrode is capacitively coupled to ground on the outside of the vacuum chamber to reduce in-

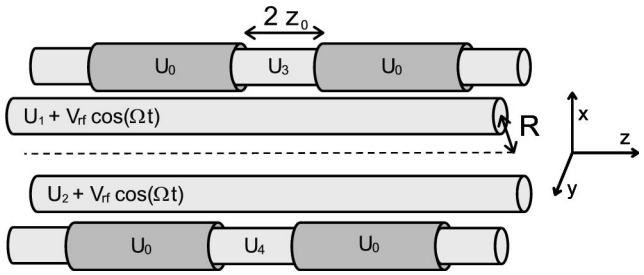

FIG. 1. Schematic diagram of the linear rf trap.

ductively coupled rf noise on their potentials. The trap is held in place by threading each end of each of the rod electrodes through one of four 0.8-mm-diam bored holes in a 4-mm-diam alumina cylinder (Alpha-Aesar Stock 32914). These cylinders are wrapped in stainless-steel shim to shield the trapping region from any potential due to charge accumulating on the alumina, although their flat ends are left exposed. In this arrangement, the closest distance from the trap axis (the dashed line in Fig. 1) to a rod surface is approximately $R=0.50$ mm. We have set the distance between the ends of the tube electrodes to approximately $2\ z_0=6$ mm.

The vacuum chamber into which this trap is placed is a Kimball Physics cylindrical vacuum chamber with eight 1.33 in. ConFlat (CF) vacuum ports along its walls and 4.5 in. CF ports on its top and bottom (model MCF450-SO20008-A). The top and bottom of this item have grooves into which two "groove grabber" clamps (Kimball Physics Part No. MCF450-GG-CA03-A) are placed on opposite sides of the chamber. The groove grabbers clamp the tops of the posts of the cage shown in Fig. 2. As shown in Fig. 2, the bottom of the cage is made from a clamping plate assembly (Kimball Physics SS-CPA-C5×7-RT1000×1600) that attaches to the bottoms of the posts. Small machined clamps are bolted to this clamping plate and in turn hold the alumina cylinders that support the trap. The trap then hangs roughly in the center of the vacuum chamber. At the top of the cage, a machined stainless-steel plate holds the imaging lens, which will be discussed in the next section. Glass viewports are connected to four of the 1.33 in. ports to accommodate two laser beams propagating $\pm 22.5°$ to the trap axis and parallel to the stainless-steel plate. Glass viewports are also placed at the top and bottom 4.5 in. ports to accommodate laser beams

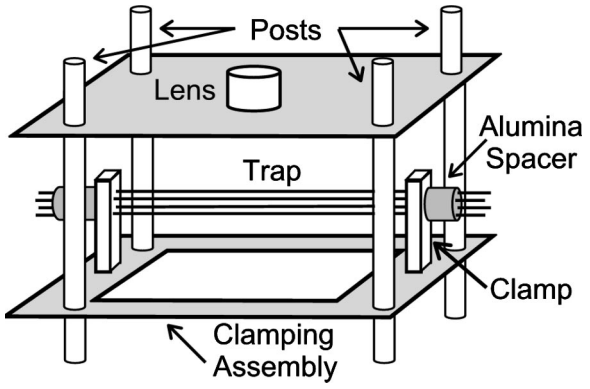

FIG. 2. Construction of the ion trap mount.

propagating perpendicular to the trap axis and to allow imaging of the trapped ions. None of these windows are antireflection coated, and no light baffling is used. The remaining 1.33 in. ports are used for electrical feedthrough connections, a pump-out port, and the strontium oven (described next). The system is pumped by a 20 l/s ion pump and a 120 l/s getter pump to 10^{-8} Pa.

Ions are formed in the trap region when neutral strontium atoms from an oven and electrons from a tungsten filament collide inside the trap. The oven is made from a single piece of 25-μm-thick tantalum foil. A section of this foil is spot welded into a 5-mm-diam tube with one open end and a slit in its middle roughly 1 mm wide and 5 mm long. Both ends of this tube terminate in 5-mm-wide, 3-cm-long strips that are spot welded to 1.0-mm-diam tantalum rods connected to an electrical feedthrough. Several mm-sized or smaller chunks of strontium metal are cut from larger pieces while in an argon atmosphere and placed into the tube through the open end, which is then crimped shut. The oven is positioned approximately 1 cm from the trap. When roughly 1.6 A runs through the oven, the long strips are heated first. The strips heat the strontium-filled tube, sending neutral strontium atoms through the trap volume. The electrons that ionize these atoms are created by a single filament that is made by winding an approximately 3 cm length of 25-μm-diam tungsten wire about a 1 mm form. This makes a filament with several loops in a length of a few mm, which is spot welded to two stainless-steel rods that are held in place by an alumina insulator identical to those holding the trap. One rod is held at potential 0 V, and the other is connected to a current limiting resistor in series with a power supply to force current through the filament. This filament is several mm behind a square of stainless-steel mesh, which is spot welded to a third rod held by the alumina insulator and held at a potential of +15 V. The mesh is about 2 cm from the trap center. Typically, 160 mA runs through the filament during the loading process, causing electrons to be stripped from its surface towards the stainless-steel mesh. Because the mesh is 50% transparent optically, many of these electrons can continue their path into the trap region. Under these conditions, each static biased electrode collects several ten's of nA of electron emission when the rf potential is applied.

III. IMAGING SYSTEM

To image the ions, an aspheric lens is positioned above the trap to collect and collimate the fluorescence from the ions, as shown in Fig. 2. This lens is an antireflection coated glass aspheric with numerical aperture N/A 0.25, produced by GelTech (lens code 350220) and sold by ThorLabs. It sits in a vacuum relieved threaded ring (also sold by ThorLabs) that is inserted in a stainless-steel plate held by the cage. The position of the lens relative to the center of the trap can be finely adjusted by rotating the threaded ring in the tapped hole in the steel plate. The drawback of this arrangement is that the position of this lens cannot be adjusted once the vacuum system has been sealed. But this arrangement simplifies the design of the optics, because the fluorescence from the ions can be collimated inside the vacuum chamber. This

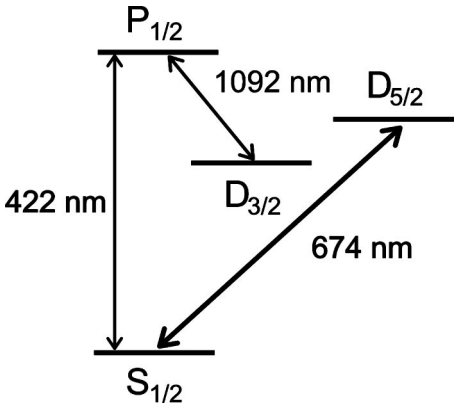

FIG. 3. Partial energy-level diagram of $^{88}Sr^{+}$.

means that subsequent optics do not have to account for refraction at the air–glass–vacuum interfaces of the top viewport.

Outside of the vacuum chamber, the light takes one of two paths. One path sends it through a 25 cm planoconvex lens that focuses the light through a rectangular aperture in front of a photon-counting photomultiplier tube (PMT). Alternatively, a removable mirror can direct the light through either a single 10 or 20 cm best-form lens or a 50 cm planoconvex lens, to focus it onto an intensified-charge-coupled-device (ICCD) camera (Princeton Instruments IMAX with blue-enhanced GEN II tube). This is by far the most expensive component of the entire experiment and could probably be replaced by a more economically priced camera. We have used geometrical optics to calculate the imaging resolution when the 50 cm lens is used and when the ions are at the focus of the aspheric lens and on its optical axis. In this ideal case, the images of the ions are nearly diffraction limited at 0.6 μm, the magnification is $\times 48$ and the ions can move along the trap axis by ± 60 μm without the image widths increasing by more than $\times 2$. When using the shorter focal length lenses, the imaging resolution is limited by the camera, which has 512×512 pixels with 35 μm effective spacing and 55 μm pixel resolution.

IV. LASER SYSTEM

Figure 3 shows a partial energy-level diagram of $^{88}Sr^{+}$ and the transitions relevant to this paper. The 422 nm $S_{1/2} \leftrightarrow P_{1/2}$ transition is the primary cooling transition. The light used to drive this transition is produced by frequency-doubling diode laser light at 844 nm in a $KNbO_3$ crystal placed in the waist of a power enhancement cavity.[17,18] The fundamental light is from a 100 mW rated 844 nm diode laser (Spectra Diode Laser SDL-5411-G1) in an extended-cavity Littrow system.[19] To phase match the second harmonic, the crystal must be held at $-17\,^{\circ}$C. This is done with two 2×2 cm thermoelectric coolers heat sunk to a copper block through which flows chilled water from a solid-state chiller. The crystal is lightly clamped in a copper block. A thin foil of indium is pressed on the crystal sides to avoid stressing the crystal and to increase thermal contact with the copper block. To keep water from condensing on the crystal, the crystal mount and copper heat sink are enclosed in a plastic tent with apertures for the light beams, desiccant is scattered about the heat sink, and dry nitrogen is flowed through the tent. The entire cavity is also enclosed in a larger tent to further keep the crystal dry.

With 7 mW of 844 nm light directed into the external cavity, up to 400 μW of 422 nm light can be sent into the trap after passing through various optics. A small fraction of the 422 nm light also passes through a heated rubidium cell to drive a transition that is nearly coincident with the $^{88}Sr^{+}$ $S_{1/2} \leftrightarrow P_{1/2}$ transition.[20,21] This helps set the laser frequency before loading ions into the trap. The 422 nm light is focused on the ions with a Gaussian waist size of 40 μm in the vertical direction and 70 μm in the horizontal direction. While loading ions and when the ions have not yet crystallized, the laser cooling is most efficient when all of the 400 μW is directed to the ions. However, we have found that 10 μW or less can efficiently cool the ions when they have crystallized.

Approximately one in 14 decays of the $P_{1/2}$ state is to the $D_{3/2}$ state. To optically pump the atoms out of the $D_{3/2}$ state, a beam of 1.1 μm light resonant with the $D_{3/2} \leftrightarrow P_{1/2}$ transition is collinearly overlapped with the 422 nm beam and focused to a waist size of 100 μm near the ions. This 1.1 μm light is produced by a Nd^{3+}-doped fiber laser[22] that has been modified from a kit purchased from FibreCore.[23] The fiber is pumped with an inexpensive 830 nm diode laser; we have used both 40 and 100 mW devices. The output power of the fiber laser is, typically, about 400 μW when a 40 mW diode laser is used, and 2.0 mW with a 100 mW pump diode laser. For tuning the laser and narrowing its frequency spectrum, an 8 mm birefringent filter is inserted into the laser cavity at Brewster's angle, and the fiber is wrapped in a polarization-controlling paddle to maintain the laser output power. Separately mounted uncoated étalons of thickness 1.0, 4.0, and 15.0 mm further narrow the laser spectrum and are adjusted for finer tuning of the laser frequency. The output coupling mirror is mounted to a ThorLabs piezostack (No. AE0203D04) to allow continuous tuning of the laser frequency. The spectrum of this laser consists of three clusters of modes. Each cluster is separated by about 600 MHz, which corresponds to the spacing between the output end of the fiber and the output coupling mirror. Within each cluster are four or five laser modes separated by about 40 MHz, corresponding to the intercavity spacing. Before any ions are trapped, the fiber laser frequency is set by driving an optogalvanic effect resonance in a strontium hollow cathode lamp. Typically, we direct 200–600 μW of 1.1 μm light into the trap.

The last transition in Fig. 3 is the 674 nm $S_{1/2} \leftrightarrow D_{5/2}$ electric dipole transition. This narrow transition can be used, for example, to observe quantum jumps[24] and to determine the ion temperature from its Doppler-broadened width. For the data presented in this article, the light used to drive this transition is produced by a 30 mW, 674 nm diode laser in an extended-cavity setup identical to that of the 844 nm diode laser. We stabilize its long-term drift and reduce its short-term frequency noise by locking it to the side of a fringe of a low-finesse ($\mathcal{F} \sim 15$) cavity. Its frequency is set by a seven-digit wave meter, after which the transition is found by scan-

ning the 674 nm laser frequency while the 422 nm light broadens the resonance. Up to 1 mW of 674 nm light can be sent to the ions after it has gone through various optics.

V. SYSTEM PERFORMANCE

To load the ions into the trap the following process is typically followed. First, the 422 nm and 1.1 μm light is directed through the geometrical center of the trap. This is found by locating the edges of the tube electrodes with the focused 422 nm beam, then setting the position of the beam between them and between the insides of the rod electrodes. The 844 nm laser frequency is detuned several hundred MHz red of the $S_{1/2}\leftrightarrow P_{1/2}$ resonance, and the fiber laser frequency is set on resonance with the $D_{3/2}\leftrightarrow P_{1/2}$ transition. To avoid coherent population trapping in the $D_{3/2}$ state, we apply to the trap region a magnetic field of several gauss perpendicular to the polarization of the 1.1 μm light.[25] To set the trap depth, approximately 100 mW of rf power is input into the resonator coil, and the voltage U_0 on the tube electrodes is typically set to 30 V. Then, about 1.6 A is flowed through the oven for 3 min. Finally, the electron filament current is set to 160 mA for 5–10 s before both the oven and filament current are turned off. Even though 422 nm bandpass filters are placed before both the PMT and the CCD camera, the light from the electron gun is too great to observe ion fluorescence during the loading process. So, the detectors are turned on only after the electron filament current is set to zero.

At this point, a large cloud of ions is usually observed with the CCD camera. The trace of the 422 nm laser beam is visible in the ion cloud as it excites the ions, and for the above loading procedure the ion cloud is usually larger than the focused laser beam. By moving the beam a known distance while observing the change in the position of its image, the magnification of the imaging system can be measured with a precision of about 20%. We find that the measurements agree with the calculated values within this uncertainty. When initially lining up the optics or searching for an ion cloud, it is easiest to use the 20 cm lens ($\times$20 magnification, 6 μm resolution) because of the greater field of view. However, with this arrangement the scattered light from the trap electrodes is more noticeable and the resolution is limited by the effective pitch of the pixels of the CCD camera. Typically, the experiment is run using the 50 cm lens to obtain higher magnification and a lower background scattering rate.

Gradually, the rf power is reduced along with the potential U_0 at the tube electrodes and the power of the cooling lasers. Some ions leave the trap, and the remaining ones become cold enough to form an ion crystal along the trap axis. We have formed linear crystals of up to 40 ions. Often, atoms that are not $^{88}Sr^+$ are contained in the ion crystals we observe. Some of these ions are likely SrH^+ and formed by collisions of Sr^+ with background hydrogen gas, and others may be formed by directly ionizing heavier background gas such as N_2, CO, or CO_2. These ions scatter no 422 nm light but are observed as apparently unoccupied sites in an ion crystal. Other ions scatter 422 nm light only weakly compared to $^{88}Sr^+$, and are likely other strontium isotopes. Crystals of only a few ions can remain in the trap as long as the cooling laser light is at least intermittently present, which can be many hours. We have not attempted to store the ions for more than 10 min without laser cooling.

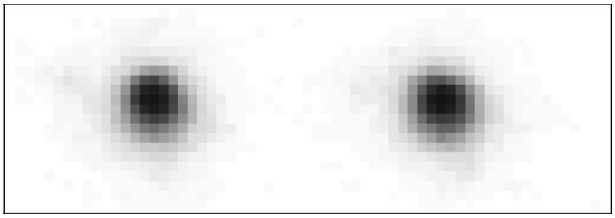

FIG. 4. Two trapped ions separated by approximately 20 μm and imaged with the ICCD camera.

Figure 4 shows an image of two $^{88}Sr^+$ ions confined in this trap, taken with the 50 cm lens in place. The image resolution in this case is 2–3 μm over an approximately 400 μm field of view. This resolution is lower than expected from the geometric optics calculations referred to above. This could be explained by the position of the aspheric lens being about 100 μm in any direction from the optimum position. Still, this performance is comparable to that of systems that include expensive multielement lenses.

We can use quantum jumps in this system to demonstrate the contrast between the background 422 nm photon scattering rate and the fluorescence rate of the ions. The fluorescence from the ions is directed onto the PMT, and all three transitions shown in Fig. 3 are driven simultaneously. When the pulses from the PMT are collected in successive 10 ms intervals, the telegraph signal typical of quantum jumps is observed as in Fig. 5. The times during which the rate of detected photons is low are when the ion is in the $D_{5/2}$ state and scattering no 422 nm photons. The average scattering rate in these periods is about 2 kHz and due to photons scattered from the trap electrodes and photons reflected from the glass viewports and diffusely scattered about the vacuum chamber. When the detected 422 nm photon rate is high, the ion is not in the $D_{5/2}$ state and is resonantly scattering 422 nm photons. During these periods, the scatter rate is 23 kHz. This value can also be used to estimate the efficiency ϵ of the imaging optics: if we conservatively assume that the total scatter rate is equal to half the decay rate $\gamma\,(=2\,\pi\times 22$ MHz) of the $P_{1/2}$ state, then $\epsilon > 3\times 10^{-4}$, comparable to other ion trapping systems.

The micromotion in this system is minimized using two methods.[16] First, the CCD camera views the ions along the

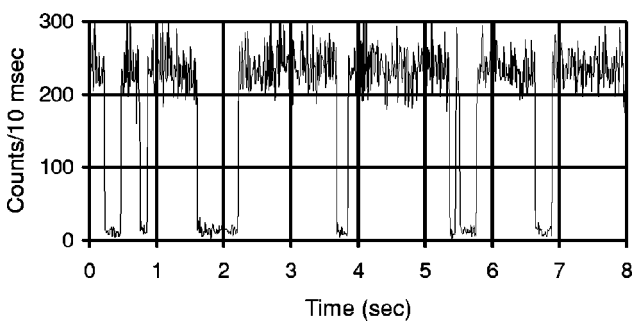

FIG. 5. Quantum jumps in $^{88}Sr^+$.

direction parallel to the y axis in Fig. 1. The rf power is raised and lowered and the bias voltages U_1 and U_3 are adjusted until the observed position of the ions in the $x-z$ plane does not change. This minimizes micromotion along the y axis. To minimize micromotion in the other two directions, the fluorescence from the ions is directed to the PMT as two 422 nm beams (propagating in the $x-z$ plane and at $\pm 22.5°$ to the z axis) alternately illuminate the ions. Then, the correlation between photon arrival times at the PMT and phase of the rf drive to the trap is measured with a Stanford Research Systems SR620 time measurement system. This instrument outputs successive histograms of relative photon arrival times, which can be integrated with a simple LabView program. The bias voltages U_1 and U_4 are adjusted until there is no measurable correlation. We find that the necessary bias voltages are several hundred mV.

We can measure the secular frequencies of the trap by driving the motional resonances with a sinusoidally varying potential applied to the oven. When the frequency of this potential is at a secular frequency of the ion motion, the image of the ion(s) greatly expands as the ion motion drastically increases. For 100 mW rf power input to the resonator, the radial secular frequency is $\omega_r/2\pi = 1.25\,\mathrm{MHz}$, and scales as expected with the rf voltage when the axial potential is small:

$$\omega_r \approx \sqrt{\frac{1}{2}}\frac{QV_{\mathrm{rf}}}{MR^2\Omega}. \tag{1}$$

Even with no voltage applied to the tube electrodes, we find that the axial secular frequency is approximately 5% of ω_r due to fringing rf fields of amplitude V_{fringe}. Applying a static potential U_0 to the tube electrodes creates an additional axial potential, so that that total axial secular frequency is

$$\omega_z = \tfrac{1}{2}\sqrt{a_z + \tfrac{1}{2}q_z^2}\,\Omega, \tag{2}$$

where

$$q_z = \frac{2QV_{\mathrm{fringe}}}{MR^2\Omega^2}, \tag{3}$$

and

$$a_z = \frac{8QU_0\kappa}{Mz_0^2\Omega^2}. \tag{4}$$

Here, κ is a shielding factor that is always less than unity, M is the ion mass, and Q is the ion charge. We find that the total axial frequency when $\omega_r/2\pi = 1.25\,\mathrm{MHz}$ and $U_0 = 45\,\mathrm{V}$ is $\omega_z/2\pi = 110\,\mathrm{kHz}$. These values give a the shielding factor $\kappa = 0.035$, which is comparable to that of other linear traps of similar dimensions.

The axial secular frequency ω_z can be significantly greater than $2\ \pi\times 100$ kHz when the potential U_0 is increased above 45 V. The axial dimension z_0 may be reduced by a factor of 2 in a future reconfiguration of the trap. According to Eq. (4), this will increase the axial secular frequency not only due to the decrease in z_0, but because the shielding factor κ should also increase when the tube electrodes are closer to the ions.

ACKNOWLEDGMENTS

It is a pleasure to thank Richard Hughes and Malcolm Boshier for useful comments on the manuscript. Daisy Raymondson constructed the 674 nm diode laser while participating in the Los Alamos Summer School, and the low-finesse cavity while part of the LANL Undergraduate Student Program.

[1] D. J. Berkeland, J. D. Miller, F. C. Cruz, B. C. Young, R. J. Rafac, X.-P. Huang, W. M. Itano, J. C. Bergquist, and D. J. Wineland, in *Atomic Physics 16*, edited by W. E. Baylis and G. W. F. Drake (AIP, Woodbury, NY, 1999), pp. 29–41.
[2] R. C. Thompson, K. Dholakia, J. L. Hernandez-Pozos, G. Z. K. Horvath, J. Rink, and D. M. Segal, Phys. Scr. **T72**, 24 (1997).
[3] A. M. Steane and D. M. Lucas, Fortschr. Phys. **48**, 839 (2000).
[4] J. D. Prestage, G. J. Dick, and L. Maleki, J. Appl. Phys. **66**, 1013 (1989).
[5] M. G. Raizen, J. M. Gilligan, J. C. Bergquist, W. M. Itano, and D. J. Wineland, Phys. Rev. A **45**, 6493 (1992).
[6] M. Block, O. Rehm, P. Seibert, and G. Werth, Eur. Phys. J. D **7**, 461 (1999).
[7] Q. A. Turchette, D. Kielpinski, B. E. King, D. Leibfried, D. M. Meekhof, C. J. Myatt, M. A. Rowe, C. A. Sackett, C. S. Wood, W. M. Itano, C. Monroe, and D. J. Wineland, Phys. Rev. A **61**, 063418 (2000).
[8] R. J. Rafac, B. C. Young, J. A. Beall, W. M. Itano, D. J. Wineland, and J. C. Bergquist, Phys. Rev. Lett. **85**, 2462 (2000).
[9] H. C. Nägerl, D. Leibfried, F. Schmidt-Kaler, J. Eschner, and R. Blatt, Opt. Express **3**, 89 (1998).
[10] R. J. Hughes, D. F. V. James, J. J. Gomez, M. S. Gulley, M. H. Holtzscheiter, P. G. Kwiat, S. K. Lamoreaux, C. G. Peterson, V. D. Sandberg, M. M. Schauer, C. M. Simmons, C. E. Thorburn, D. Tupa, P. Z. Wang, and A. G. White, Fortschr. Phys. **46**, 329 (1998).
[11] M. E. Poitzsch, J. C. Bergquist, W. M. Itano, and D. J. Wineland, Rev. Sci. Instrum. **67**, 129 (1996).
[12] K. Toyoda, H. Kataoka, Y. Kai, A. Miura, M. Watanabe, and S. Urabe, Appl. Phys. B: Lasers Opt. **72**, 327 (2001).
[13] U. Tanaka, H. Imajo, K. Hayasaka, R. Ohmukai, M. Watanabe, and S. Urabe, Opt. Lett. **22**, 1353 (1997).
[14] P. A. Barton, C. J. S. Donald, D. M. Lucas, D. A. Stevens, A. M. Steane, and D. N. Stacey, Phys. Rev. A **62**, 032503 (2000).
[15] W. W. Macaplin and R. O. Schildknecht, Proc. IRE **47**, 2099 (1959).
[16] D. J. Berkeland, J. D. Miller, J. C. Bergquist, W. M. Itano, and D. J. Wineland, J. Appl. Phys. **83**, 5025 (1998).
[17] P. Lodahl, J. L. Sørensen, and E. S. Polzik, Appl. Phys. B: Lasers Opt. **B64**, 383 (1997).
[18] M. K. Chun, L. Goldberg, and J. F. Weller, Appl. Phys. Lett. **53**, 1170 (1988).
[19] A. S. Arnold, J. S. Wilson, and M. G. Boshier, Rev. Sci. Instrum. **69**, 1236 (1998).
[20] M. Musha, A. Zvyagin, K. Nakagawa, and M. Ohtsu, Jpn. J. Appl. Phys. **33**, 1603 (1994).
[21] A. A. Madej, L. Marmet, and J. E. Bernard, Appl. Phys. B: Lasers Opt. **B67**, 229 (1998).
[22] A. A. Madej, W. E. Berger, and G. R. Hanes, Opt. Commun. **73**, 147 (1989).
[23] FLK1000S neodymium-doped fiber laser kit from FiberCore, Ltd., Epsilon House, Chilworth Research Centre, Southampton, Hampshire, U.K. SO16 7NS.
[24] R. J. Cook, in *Progress in Optics XXVIII*, edited by E. Wolf (North-Holland, Amsterdam, 1990), pp. 362–416.
[25] D. J. Berkeland and M. G. Boshier, Phys. Rev. A **65**, 033413 (2002).